PCCP

PAPER

View Article Online
View Journal | View Issue

Cite this: *Phys. Chem. Chem. Phys.*, 2019, **21**, 25215

Aromatic character of $[Au_{13}]^{5+}$ and $[MAu_{12}]^{4+/6+}$ (M = Pd, Pt) cores in ligand protected gold nanoclusters – interplay between spherical and planar σ-aromatics†

Nikita Fedik,[a] Alexander I. Boldyrev *[a] and Alvaro Muñoz-Castro *[b]

Received 12th August 2019,
Accepted 17th October 2019

DOI: 10.1039/c9cp04477a

rsc.li/pccp

The most characteristic feature of planar π-aromatics is the ability to sustain a long-range shielding cone under a magnetic field oriented in a specific direction. In this article, we showed that similar magnetic responses can be found in σ-aromatic and spherical aromatic systems. For $[Au_{13}]^{5+}$, long-range characteristics of the induced magnetic field in the bare icosahedral core are revealed, which are also found in the ligand protected $[Au_{25}(SH)_{18}]^{-}$ model, proving its spherical aromatic properties, also supported by the AdNDP analysis. Such properties are given by the 8-ve of the structural core satisfying the Hirsch $2(N + 1)^2$ rule, which is also found in the isoelectronic $[M@Au_{12}]^{4+}$ core, a part of the $[MAu_{24}(SR)_{18}]^{2-}$ (M = Pd, Pt) cluster. This contrasts with the $[M@Au_{12}]^{6+}$ core in $[MAu_{24}(SR)_{18}]^{0}$ (M = Pd, Pt), representing 6-ve superatoms, which exhibit characteristics of planar σ-aromatics. Our results support the spherical aromatic character of stable superatoms, whereas the 6-ve intermediate electron counts satisfy the $4N + 2$ rule (applicable for both π- and σ-aromatics), showing the reversable and controlled interplay between 3D spherical and 2D σ-aromatic clusters.

Introduction

Since the early characterization of thiolate-protected gold nanoclusters,[1] considerable efforts have been made driven by their potential role as efficient building blocks for functional nanomaterials.[2–11] Currently, synthetic methods are able to achieve atomically-precise clusters.[12,13] It became possible to render relevant structures at nanosized domains (<2 nm) to study the evolution from small aggregates to nanocrystals. Their molecule-like bandgap[14–17] and novel properties are useful towards promising applications in catalysis, sensing, and biomedicine among others.[10,11,18–24]

Amidst the different thiolate-protected gold clusters, $Au_{25}(SR)_{18}$ is one of the most prominent members,[25] displaying high stability against degradation. This remarkable stability originates from both geometric and electronic characteristics.[6,26–29] Its structure is composed of a formal $[Au_{13}]^{5+}$ core unit with 8-valence electrons (ve),[7,17] ensuring the occupancy of S and P superatomic electronic shells in its anionic $[Au_{25}(SR)_{18}]^{-}$ form.[30–32] Such an electronic configuration resembles the one of noble gas atoms and is responsible for their unprecedented stability. Further doping of Au_{25} with Pd and Pt located at the endohedral site improves the cluster versatility resulting in $M@Au_{24}(SR)_{18}$ species[33,34] characterized in both dianionic and neutral charge states. This enables interconversion between 8- and 6-ve superatomic clusters.[35] Interestingly, the 8-ve count also fulfills the $2(N + 1)^2$ Hirsch rule for spherical aromatic structures as an extension of the classical $(4N + 2)$ Hückel rule.[36,37] The Hirsch rule[36–39] recognizes three-dimensional molecules having patterns similar to classic two-dimensional aromatic species known for their remarkable stability.

However, the language that the community uses to discuss spherical aromatic structures is not completely settled, and in the literature, they are sometimes referred to as superatoms (due to the resemblance of their bond shapes to the atomic orbitals) or 3D aromatics as was initially proposed by Lipscomb. To overcome any terminology discrepancies, we would like to explicitly specify that all these terms are absolutely interchangeable and describe the same phenomenon.[40,41]

Recently, we have extended the approach of magnetic criteria of aromaticity, providing another reliable method for studying spherical aromatic clusters based on their long-range magnetic behavior owing to the formation of a shielding cone in analogy to planar aromatics, as a common property.[42] This approach is not influenced by the local response from each face in the spherical

[a] *Department of Chemistry and Biochemistry, Utah State University, 0300, Old Main Hill, Logan, Utah, 84322-0300, USA. E-mail: a.i.boldyrev@usu.edu*
[b] *Grupo de Química Inorgánica y Materiales Moleculares, Facultad de Ingenieria, Universidad Autonoma de Chile, El Llano Subercaseaux 2801, Santiago, Chile*

† Electronic supplementary information (ESI) available. See DOI: 10.1039/c9cp04477a

cage due to its focus on long-range behavior, which is more critical in heavy-elements.[43]

Herein, we obtained further understanding of stable gold clusters based on $[Au_{13}]^{5+}$ considering their spherical aromatic features. Also, we analyzed $[M@Au_{12}]^{4+}$ and $[M@Au_{12}]^{6+}$ cores observed in $[MAu_{24}(SR)_{18}]^{2-}$ and $[MAu_{24}(SR)_{18}]^{0}$ (M = Pd and Pt) and showed that they could be denoted as 8- and 6-ve superatoms, respectively.

Computational details

We deciphered their bonding patterns *via* adaptive natural density partitioning (AdNDP) analysis,[44] which combines the concepts of localized and delocalized bonding crucial for solving complicated cases.[45–49] Magnetic response properties were also calculated to discuss the aromatic character of clusters. Isosurfaces of the induced magnetic field were obtained as a three-dimensional grid of shielding tensor (σ_{ij}) given in ppm, with $B_i^{ind} = -\sigma_{ij}B_j^{ext}$,[50–54] depending on different representative orientations of the external field (B^{ext}) with respect to i and j suffixes. They relate to the x-, y- and z-axes. These effects were considered within the GIAO formalism, employing the Perdew, Burke and Ernzerhof[55,56] (OPBE-GGA) functional and triple-ξ Slater basis set plus the double-polarization (STO-TZ2P) basis set. Relativistic effects were taken into account *via* the ZORA Hamiltonian.[57] All calculations including structure optimization were performed using relativistic DFT methods using the ADF 2016 code.[58] Relaxed structures were obtained at the TZ2P-PBE/ZORA level. Steps necessary to perform AdNDP analysis were carried out in Gaussian16[59] utilizing the PBE0/def2-SVP level of theory.[60]

Results and discussion

Spherical aromatic compounds have attracted a lot of attention and represent an interesting extension to the concept of aromaticity, historically applied to π-planar organic structures. This relevant extension recognizes three-dimensional molecules whose bonding pattern and stability resemble those of two-dimensional aromatic species.[36–39] Among the studied thiolate-protected gold nanoparticles, $[Au_{25}(SR)_{18}]^{-}$ is one of the most prominent examples, providing a prototypical structure to evaluate properties of stable clusters. Its inner core is formally viewed as a $[Au_{13}]^{5+}$ cluster (Fig. 1) protected by a layer of organic ligands. The bare $[Au_{13}]^{5+}$ cluster retains an icosahedral structure in contrast to the neutral counterpart, showing lower symmetry.[60–64]

The magnetic criteria of aromaticity[54,65–67] have been well employed to evaluate spherical aromatic hollow cages,[66,68] which are not straight in endohedral systems such as Au_{13} and MAu_{12} cores, where a central probe is highly influenced by the inner atom. To overcome such inconvenience, we focus on long-range characteristics of the induced magnetic field in bare $[Au_{13}]^{5+}$, $[Pd@Au_{12}]^{4+}$ and $[Pd@Au_{12}]^{6+}$.

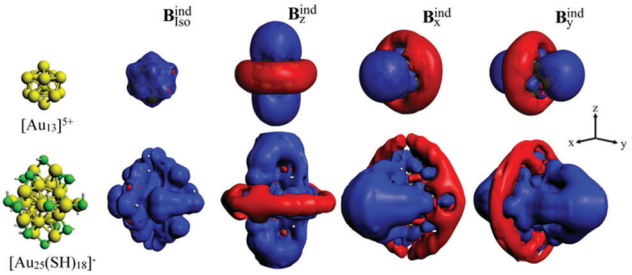

Fig. 1 Magnetic response properties of $[Au_{13}]^{5+}$ and $[Au_{25}(SH)_{18}]^{-}$, denoting the response under different orientations of the external field (B_z^{ind}, B_x^{ind}, and B_y^{ind}) and their isotropic (averaged) term (B_{iso}^{ind}). Isosurfaces set to ±3 ppm, blue means shielding; red means deshielding.

The isotropic response ($B_{iso}^{ind} = -(1/3)(\sigma_{xx} + \sigma_{yy} + \sigma_{zz})B^{ext}$) accounts for the orientational averaged behavior under a constant motion situation, such as in solution state (also denoted as NICS[59]). In Fig. 1, the obtained B_{iso}^{ind} for $[Au_{13}]^{5+}$ exhibits a continuous shielding region indicating the formation of currents. These currents generate a magnetic field that opposes the external field[69] (a 'diatropic' current) ruling the magnetic response of such a cluster core. At distances of 8.5 Å from the center, a shielding value of 3.0 ppm is observed. At the inner section of the core, shielding values > -45.0 ppm are found, owing to the presence of the endohedral gold atom, whereas the hollow isoelectronic cage $[Au_{12}]^{4+}$ depicts values of −35.0 ppm at the center. As has been shown for Hirsch's aromatic fullerenes, the formation of a shielding cone is parallel to the orientation of the applied field.[42] Interestingly, such features remain in the overall ligand-protected $[Au_{25}(SH)_{18}]^{-}$ cluster. These results support that the cluster-core features remain in the overall structure with a slight extension of the shielding cone owing to the contribution from the ligand-protecting layer (3 ppm–10.0 Å). Thus, hereafter, we focus our effort on determining the magnetic response characteristics of MAu_{12} cluster cores.

To further confirm aromaticity, adaptive natural density partitioning (AdNDP) analysis was employed. The AdNDP analysis for $[Au_{13}]^{5+}$ shows a set of four delocalized 13c–2e bonds in agreement with the 8-ve count fulfilling a $1S^21P^6$ electronic shell structure, satisfying the Hirsch rule for spherical aromatic compounds (Fig. 2). This picture agrees with the molecular orbitals accounting for the superatomic 1S and 1P shells (Fig. S1, ESI†). The same holds when the ligand layer is taken into account in $[Au_{25}(SH)_{18}]^{-}$, where the related set of four 25c–2e delocalized bonds supports the extension of the spherical aromatic properties from the bare core to the overall ligand-protected architecture. In addition, five localized lone pairs on every gold atom were located because of the complete occupancy of the $5d^{10}$-Au shell (Fig. S2, ESI†). The aromatic character of the $[Au_{13}]^{5+}$ cluster core originates from the favorable $1S^21P^6$ electronic configuration, unraveling that the enhanced stability observed for $[Au_{25}(SR)_{18}]^{-}$ clusters involves an aromatic behavior.

Further inclusion of dopant atoms was shown to increase the versatility of such species, resulting in more tailorable clusters.[33,34] For the 8-ve monodoped cores $[M@Au_{12}]^{4+}$, it is

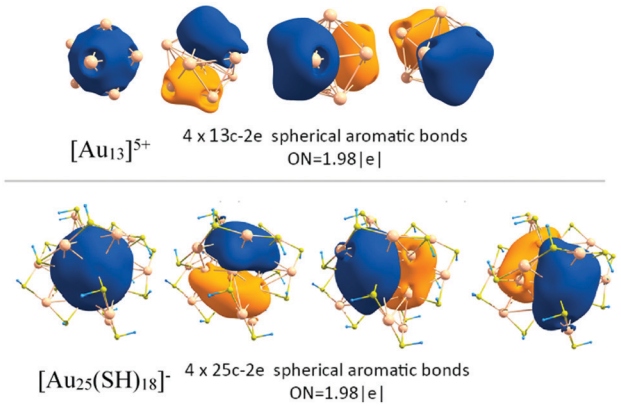

Fig. 2 Chemical bonding pattern for $[Au_{13}]^{5+}$ and $[Au_{25}(SH)_{18}]^{-}$, as shown by the AdNDP analysis. ON stands for occupation number.

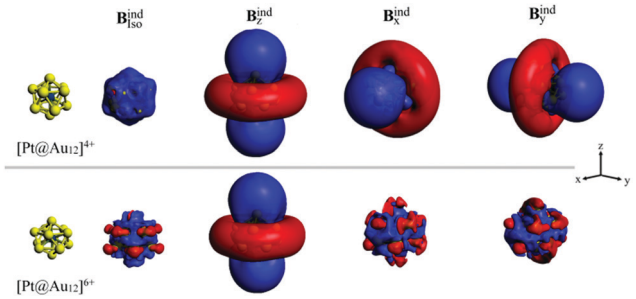

Fig. 3 Magnetic response properties of the representative $[PtAu_{12}]^{6+}$ and $[PtAu_{12}]^{4+}$ cores. Isosurfaces set to ±3 ppm, blue means shielding; red means deshielding.

found that they are able to sustain the formation of a shielding cone upon an external field at different orientations (Fig. 3), which averages together to form a continuous shielding region. Such features resemble the behavior found in $[Au_{13}]^{5+}$ supported by the formation of shielding cone characteristics in several orientations owing to its inherent three-dimensional aromatic properties, as was observed for spherical aromatic fullerenes.[70–72] Obviously, these properties can be extended to the related ligand-protected $[MAu_{24}(SR)_{18}]^{2-}$ containing the $[M@Au_{12}]^{4+}$ core. The AdNDP analysis shows a consequent set of four delocalized 13c–2e bonds satisfying the Hirsch rule meaning a similar bonding pattern between isoelectronic $[M@Au_{12}]^{4+}$ and $[Au_{13}]^{5+}$ cores enabling the spherical aromatic character (Fig. 4 and Fig. S3, S5, ESI†). Moreover, the icosahedral structure of the $[Au_{13}]^{5+}$ core is preferred by the herein discussed spherical aromatic characteristics.

Note, reversible interconversion between neutral and dianionic species has been shown for $MAu_{24}(SR)_{18}$ clusters, as proven by cyclic voltammetry among other experiments.[35] This provides a way to control a 6-ve ↔ 8-ve variation of electronic structure in both monopalladium and monoplatinum structures. As a consequence, the nearly spherical icosahedral 8-ve MAu_{12} core is distorted leading to a flattened cage in its 6-ve form.[35] In turn, it splits the parent $1S^21P^6$ shell after the removal of two electrons in $1S^21P^4_{x,y}$ and $1P^0_z$ denoted as the HOMO and LUMO, respectively, in the $[MAu_{12}]^{6+}$ core.

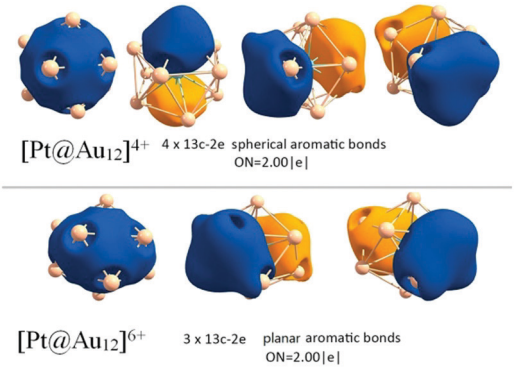

Fig. 4 Chemical bonding pattern for $[PtAu_{12}]^{4+}$ and $[PtAu_{12}]^{6+}$, as shown by the AdNDP analysis. ON stands for occupation number.

For such 6-ve species, it is interesting to evaluate if the aromatic properties are preserved or not, when the electron count deviates from that expected by the $2(N + 1)^2$ Hirsch rule. Is it possible to find any resemblance of spherical aromatics despite the unfavorable electron count? Indeed, the AdNDP analysis for $[MAu_{12}]^{6+}$ shows now only three-sets of 13c–2e delocalized bonds (Fig. 4 and Fig. S4, S6, ESI†), accounting for its $1S^21P^4_{x,y}$ superatomic 2D-shell structure involving all the bare core atoms. It denotes a non-spherical aromatic character in this three dimensional structure. Alternatively, we also localized the density only on a Au_{10} ribbon and got a set of three bonds having proper symmetry (Fig. S7, ESI†) but unreasonably low ONs in the range 1.15–0.54|*e*|. We believe that these results fully confirm that in order to construct delocalized bonds and bear aromatic properties (either 2D or 3D), contributions from all atoms are essential.

However, the experimentally demonstrated preference of neutral charge state of $[MAu_{24}(SR)_{18}]^{0}$ clusters bearing 6-ve cluster cores[35] over the expected 8-ve $[MAu_{24}(SR)_{18}]^{2-}$ spherical aromatic species suggests the pronounced reminiscence of aromatic properties in the $[MAu_{12}]^{6+}$ cores. To evaluate such behavior, we unraveled the characteristics of the induced magnetic field.

Interestingly, the shielding cone properties observed for spherical aromatic cores are no longer available with the striking exception of the external field oriented perpendicularly to the plane where $1P_x$ and $1P_y$ orbitals form the superatomic electronic shells (Fig. 3). For other representative directions (along the *x*- and *y*-axis), a short-ranged response is found, which after averaging displays both shielding and deshielding regions as can be seen from its B^{ind}_{iso} isosurface, which further confirms the non-spherical aromatic character for 6-ve $[MAu_{12}]^{6+}$ cores. Moreover, the capability to sustain a shielding cone property upon a parallelly oriented field strongly resembles the behavior of par excellence aromatic molecules upon different orientations of the field.[73,74] Benzene sustains a shielding cone property when the field is parallelly oriented to the molecular plane (along *z*-axis), denoting a short-ranged response for *x*- and *y*-orientations.[73] However, we believe that the investigated $[MAu_{12}]^{6+}$ core is an extraordinary case of σ-aromaticity in gold clusters. The aromatic bonds are constructed from superatomic valence shell $1S^21P^4_{x,y}$

which fully correlates with their shape. The first bond from the set of three 13c–2e has no nodal plane whereas the other two have one nodal plane each meaning that they are formed from the parental P orbitals. This contrasts to the canonical π-aromatics like benzene in which all three aromatic bonds have one nodal plane and resemble P orbitals. Note that σ-aromaticity was initially proposed for Li and Mg clusters by Alexandrova and Boldyrev,[75] but recently it was experimentally confirmed and shown to exist even in the bottled compound $C_6(SePh)_6^{2+}$ by Saito and co-workers.[76]

Thus, our results reveal that the 6-ve $[MAu_{12}]^{6+}$ core from $[MAu_{24}(SR)_{18}]^0$ species, bearing three 13c–2e delocalized bonds, exhibits an unprecedented planar σ-aromatic behavior for quasi-spherical cages. Obviously, it confirms the presence of planar σ-aromatic species in the field of ligand-protected gold clusters. These planar aromatic characteristics support the preferred stability of 6-ve $[MAu_{24}(SR)_{18}]^0$ and the further reversible 6-ve ↔ 8-ve interconversion. Moreover, it enables a controlled shift between planar σ-aromatics and Hirsch's three-dimensional aromatics fulfilling $(4N + 2)$ and $2(N + 1)^2$ rules, respectively. Therefore, planar σ-aromatic cores can be further manipulated electrochemically in order to deliver spherical aromatic species in doped clusters derived from the $Au_{25}SR_{18}$ superatom. Overall, superatomic clusters are shown to have inherent and versatile features to sustain both spherical and planar σ-aromatic characteristics that can be controlled by tuning of their charge states. Moreover, this aromaticity discussion prompts intriguing questions of what kind of aromatics is the 18-ve gold core, fulfilling both $4N + 2$ and $(2N + 1)^2$ rules, and we aim to answer them in our future study.

Conclusions

Here, we have revealed and confirmed the inherent spherical aromatic properties of the superatomic 8-electron $Au_{25}(SR)_{18}^-$ clusters ascribed to their inner $[Au_{13}]^{5+}$ core, by the capabilities to sustain a shielding cone property upon different orientations of the applied field, as it is a characteristic of Hirsch aromatics. The 8-ve count leads to a set of four 13c–2e delocalized orbitals accounting for the $1S^21P^6$ superatomic electronic shell. Such features are also observed in the Pd and Pt monodoped 8-ve $[MAu_{12}]^{4+}$ cores found in $MAu_{24}(SR)_{18}^{2-}$, supporting the spherical aromatic behavior in other superatomic cores. By contrast, the 6-ve cluster core from preferred $MAu_{24}(SR)_{18}^0$ species denotes a set of three 13c–2e delocalized orbitals leading to a shielding cone property reserved only for a perpendicularly oriented field about the plane where $1P_x$ and $1P_y$ shells lie, which is an inherent feature for planar aromatics. Thus, the behavior of 6-ve $[MAu_{12}]^{6+}$ cores is the first result showcasing the formation of planar σ-aromatics in quasi-spherical clusters owing to its $1S^21P^4_{x,y}$ superatomic electronic shell.

Conflicts of interest

There are no conflicts to declare.

Acknowledgements

This project was supported by the National Science Foundation (CHE-1664379 to A. I. B.). A. M.-C. acknowledges financial support from FONDECYT 1180683.

Notes and references

1 M. Brust, M. Walker, D. Bethell, D. J. Schiffrin and R. Whyman, *Chem. Commun.*, 1994, 801–802.
2 H. Qian, Y. Zhu and R. Jin, *ACS Nano*, 2009, **3**, 3795–3803.
3 R. L. Whetten, J. T. Khoury, M. M. Alvarez, S. Murthy, I. Vezmar, Z. L. Wang, P. W. Stephens, C. L. Cleveland, W. D. Luedtke and U. Landman, *Adv. Mater.*, 1996, **8**, 428–433.
4 L. A. Oro, P. Braunstein and P. R. Raithby, *Metal clusters in chemistry*, Wiley-VCH, Weinheim, Germany, 1999, vol. 3.
5 M.-C. Daniel and D. Astruc, *Chem. Rev.*, 2004, **104**, 293–346.
6 M. W. Heaven, A. Dass, P. S. White, K. M. Holt and R. W. Murray, *J. Am. Chem. Soc.*, 2008, **130**, 3754–3755.
7 M. Walter, J. Akola, O. Lopez-Acevedo, P. D. Jadzinsky, G. Calero, C. J. Ackerson, R. L. Whetten, H. Grönbeck, H. Häkkinen, H. Gronbeck and H. Hakkinen, *Proc. Natl. Acad. Sci. U. S. A.*, 2008, **105**, 9157–9162.
8 P. Jena, *J. Phys. Chem. Lett.*, 2013, **4**, 1432–1442.
9 S. Knoppe, I. Dolamic and T. Bürgi, *J. Am. Chem. Soc.*, 2012, **134**, 13114–13120.
10 Y. Levi-Kalisman, P. D. Jadzinsky, N. Kalisman, H. Tsunoyama, T. Tsukuda, D. A. Bushnell and R. D. Kornberg, *J. Am. Chem. Soc.*, 2011, **133**, 2976–2982.
11 J. M. Galloway, J. P. Bramble, A. E. Rawlings, G. Burnell, S. D. Evans and S. S. Staniland, *Small*, 2012, **8**, 204–208.
12 R. Jin, *Nanoscale*, 2015, **7**, 1549–1565.
13 M. Zhu, C. M. Aikens, F. J. Hollander, G. C. Schatz and R. Jin, *J. Am. Chem. Soc.*, 2008, **130**, 5883–5885.
14 R. Jin, *Nanoscale*, 2010, **2**, 343–362.
15 A. Dass, R. Guo, J. B. Tracy, R. Balasubramanian, A. D. Douglas and R. W. Murray, *Langmuir*, 2008, **24**, 310–315.
16 R. Tsunoyama, H. Tsunoyama, P. Pannopard, J. Limtrakul and T. Tsukuda, *J. Phys. Chem. C*, 2010, **114**, 16004–16009.
17 H. Häkkinen, *Chem. Soc. Rev.*, 2008, **37**, 1847–1859.
18 T. Tsukuda, H. Tsunoyama and H. Sakurai, *Chem. – Asian J.*, 2011, **6**, 736–748.
19 Y. Zhu, H. Qian and R. Jin, *J. Mater. Chem.*, 2011, **21**, 6793–6799.
20 K. Kwak, S. S. Kumar and D. Lee, *Nanoscale*, 2012, **4**, 4240–4246.
21 N. Sakai and T. Tatsuma, *Adv. Mater.*, 2010, **22**, 3185–3188.
22 Z. Wu, M. Wang, J. Yang, X. Zheng, W. Cai, G. Meng, H. Qian, H. Wang and R. Jin, *Small*, 2012, **8**, 2028–2035.
23 R. W. Murray, *Chem. Rev.*, 2008, **108**, 2688–2720.
24 G. Guan, S.-Y. Zhang, Y. Cai, S. Liu, M. S. Bharathi, M. Low, Y. Yu, J. Xie, Y. Zheng, Y.-W. Zhang and M.-Y. Han, *Chem. Commun.*, 2014, **50**, 5703.
25 X. Kang, H. Chong and M. Zhu, *Nanoscale*, 2018, **10**, 10758–10834.
26 O. Toikkanen, V. Ruiz, G. Rönnholm, N. Kalkkinen, P. Liljeroth and B. M. Quinn, *J. Am. Chem. Soc.*, 2008, **130**, 11049–11055.

27 H. Qian, C. Liu and R. Jin, *Sci. China: Chem.*, 2012, **55**, 2359–2365.
28 P. Maity, S. Xie, M. Yamauchi and T. Tsukuda, *Nanoscale*, 2012, **4**, 4027–4037.
29 H. Häkkinen, *Nat. Chem.*, 2012, **4**, 443–455.
30 S. N. Khanna and P. Jena, *Phys. Rev. B: Condens. Matter Mater. Phys.*, 1995, **51**, 13705–13716.
31 D. Jiang and S. Dai, *Inorg. Chem.*, 2009, **48**, 2720–2722.
32 F. K. Sheong, J.-X. Zhang and Z. Lin, *Inorg. Chem.*, 2016, **55**, 11348–11353.
33 H. Qian, D. Jiang, G. Li, C. Gayathri, A. Das, R. R. Gil and R. Jin, *J. Am. Chem. Soc.*, 2012, **134**, 16159–16162.
34 Y. Niihori, W. Kurashige, M. Matsuzaki and Y. Negishi, *Nanoscale*, 2013, **5**, 508–512.
35 K. Kwak, Q. Tang, M. Kim, D. Jiang and D. Lee, *J. Am. Chem. Soc.*, 2015, **137**, 10833–10840.
36 Z. Chen, H. Jiao, A. Hirsch and W. Thiel, *J. Mol. Model.*, 2001, **7**, 161–163.
37 A. Hirsch, Z. Chen and H. Jiao, *Angew. Chem., Int. Ed.*, 2000, **39**, 3915–3917.
38 M. Bühl and A. Hirsch, *Chem. Rev.*, 2001, **101**, 1153–1184.
39 J. Aihara, *J. Am. Chem. Soc.*, 1978, **100**, 3339–3342.
40 N. Fedik, M. Kulichenko and A. I. Boldyrev, *Chem. Phys.*, 2019, **522**, 134–137.
41 C. Liu, N. V. Tkachenko, I. A. Popov, N. Fedik, X. Min, C.-Q. Xu, J. Li, J. E. McGrady, A. I. Boldyrev and Z.-M. Sun, *Angew. Chem., Int. Ed.*, 2019, **58**, 8367–8371.
42 A. Muñoz-Castro, *Phys. Chem. Chem. Phys.*, 2017, **19**, 12633–12636.
43 A. Muñoz-Castro, *J. Phys. Chem. C*, 2012, **116**, 17197–17203.
44 D. Y. Zubarev and A. I. Boldyrev, *J. Phys. Chem. A*, 2009, **113**, 866–868.
45 M. Kulichekno, N. Fedik, K. V. Bozhenko and A. I. Boldyrev, *J. Phys. Chem. B*, 2019, **123**, 4065–4069.
46 G. Liu, N. Fedik, C. Martinez-Martinez, S. M. Ciborowski, X. Zhang, A. I. Boldyrev and K. H. Bowen, *Angew. Chem., Int. Ed.*, 2019, **58**, 13789–13793.
47 M. Kulichekno, N. Fedik and K. V. Bozhenko, *Chem. – Eur. J.*, 2019, **25**, 5311–5315.
48 N. V. Tkachenko, D. Steglenko, N. Fedik, N. M. Boldyreva, R. M. Minyaev, V. I. Minkin and A. I. Boldyrev, *Phys. Chem. Chem. Phys.*, 2019, **21**, 19764–19771.
49 O. A. Gapurenko, R. M. Minyaev, N. S. Fedik, V. V. Koval, A. I. Boldyrev and V. I. Minkin, *Struct. Chem.*, 2019, **30**, 805–814.
50 M. Baranac-Stojanović, *RSC Adv.*, 2014, **4**, 308–321.
51 S. Klod and E. Kleinpeter, *J. Chem. Soc., Perkin Trans. 2*, 2001, 1893–1898.
52 N. D. Charistos, A. G. Papadopoulos and M. P. Sigalas, *J. Phys. Chem. A*, 2014, **118**, 1113–1122.
53 T. Heine, C. Corminboeuf and G. Seifert, *Chem. Rev.*, 2005, **105**, 3889–3910.
54 R. Islas, T. Heine and G. Merino, *Acc. Chem. Res.*, 2012, **45**, 215–228.
55 J. P. Perdew, K. Burke and Y. Wang, *Phys. Rev. B: Condens. Matter Mater. Phys.*, 1996, **54**, 16533–16539.
56 J. P. Perdew, K. Burke and M. Ernzerhof, *Phys. Rev. Lett.*, 1996, **77**, 3865–3868.
57 S. K. Wolff, T. Ziegler, E. van Lenthe and E. J. Baerends, *J. Chem. Phys.*, 1999, **110**, 7689.
58 Amsterdam Density Functional (ADF 2016) Code, Vrije Universiteit: Amsterdam, The Netherlands. Available at: http://www.scm.com.
59 M. J. Frisch, G. W. Trucks, H. B. Schlegel, G. E. Scuseria, M. A. Robb, J. R. Cheeseman, G. Scalmani, V. Barone, G. A. Petersson *et al.*, *Gaussian 16, Revision C.01*, Gaussian, Inc., Wallingford CT, 2016.
60 F. Weigland and R. Ahlrichs, *Phys. Chem. Chem. Phys.*, 2005, **7**, 3297–3305.
61 M. Gruber, G. Heimel, L. Romaner, J.-L. Brédas and E. Zojer, *Phys. Rev. B: Condens. Matter Mater. Phys.*, 2008, **77**, 165411.
62 B. Assadollahzadeh and P. Schwerdtfeger, *J. Chem. Phys.*, 2009, **131**, 064306.
63 L. Xiao, B. Tollberg, X. Hu and L. Wang, *J. Chem. Phys.*, 2006, **124**, 114309.
64 M. P. Johansson, I. Warnke, A. Le and F. Furche, *J. Phys. Chem. C*, 2014, **118**, 29370–29377.
65 R. Gershoni-Poranne and A. Stanger, *Chem. Soc. Rev.*, 2015, **44**, 6597–6615.
66 A. C. Castro, E. Osorio, J. O. C. Jimenez-Halla, E. Matito, W. Tiznado and G. Merino, *J. Chem. Theory Comput.*, 2010, **6**, 2701–2705.
67 G. Merino, A. Vela and T. Heine, *Chem. Rev.*, 2005, **105**, 3812–3841.
68 T. Ishida, H. Kanno and J. Aihara, *Bull. Chem. Soc. Jpn.*, 2007, **80**, 2145–2148.
69 J. A. N. F. Gomes and R. B. Mallion, *Chem. Rev.*, 2001, **101**, 1349–1384.
70 A. Muñoz-Castro and R. B. King, *Inorg. Chem.*, 2017, **56**, 15251–15258.
71 N. D. Charistos and A. Muñoz-Castro, *J. Phys. Chem. C*, 2018, **122**, 9688–9698.
72 A. Muñoz-Castro, *Chem. Commun.*, 2015, **51**, 10287–10290.
73 A. G. Papadopoulos, N. D. Charistos and A. Muñoz-Castro, *ChemPhysChem*, 2017, **18**, 1499–1502.
74 P. R. von Schleyer and H. Jiao, *Pure Appl. Chem.*, 1996, **68**, 209–218.
75 A. N. Alexandrova and A. I. Boldyrev, *J. Phys. Chem. A*, 2003, **107**, 554–560.
76 S. Furukawa, M. Fujita, Y. Kanatomi, M. Minoura, M. Hatanaka, K. Morokuma, K. Ishimura and M. Saito, *Commun. Chem.*, 2018, **1**, 60.